Available online at www.sciencedirect.com

ScienceDirect

Journal of Sound and Vibration 308 (2007) 563–578

JOURNAL OF SOUND AND VIBRATION

www.elsevier.com/locate/jsvi

Shock response spectrum in plates under impulse loads

Fabio Botta*, Giovanni Cerri

Dipartimento di Ingegneria Meccanica e Industriale, Università degli Studi di Roma Tre, Roma, Italy

Accepted 2 April 2007
The peer review of this article was organised by the Guest Editor
Available online 2 July 2007

Abstract

In this paper, the study of a plate under impulse loads and the correlated Shock Response Spectrum (SRS) has been carried out. The Reissner–Mindlin plate have been considered and the modal analysis technique used to develop the solution. The influence of the impulse (rise function, rise time) and geometric parameters (thickness of the plate, distance of the measure point from the point load) has been evaluated.

1. Introduction

A response of an elastic plate to impulse loads is of paramount interest in wide ranges of structural analysis concerning mechanical, aerospace, military and civil engineering, particularly for applications. For example, in aerospace applications, impulses initiated by pyrotechnic devices appear in different places during and after the launch of a satellite (due to launch vehicle, separation, deployment of appendages such as solar arrays and antennas). The firings of these pyrotechnical charges generate severe impulse loads (so-called pyroshock), which may cause failures, especially in electronic and electromechanical equipments [1]. Because of the complexity of structures it is difficult to describe the shock transmission and to predict the shock level as well as structural failure. To overcome this difficulty, engineers have found most useful the Shock Response Spectrum concept (SRS)[1] (see Appendix). Studies in this field are of two types: some analyze the possibility of reproducing the real SRS in laboratory [3–6], others, instead, analyze the behavior of structures under impulse loads [7,8]. In the first case aerospace industries, for example, replicate the real shock loads in a laboratory, where the test item is attached on an aluminum plate [3]. The plate is struck with an impactor, and the SRS is evaluated by the accelerations measured near the test item. The optimal configuration of the system is obtained by trial and error method, varying the plate parameters (width, thickness, etc.) or the impulse parameters (intensity, point load, material of the impactor, etc.) until the obtained SRS is "near" the real SRS. In the second case, the analysis can be carried out by using the exact three-dimensional (3D) theory or one of the approximate models for plates, that is derived from that theory introducing some limitations on the kinematics (Kirchhoff–Love, Reissner–Mindlin, etc.). In this paper a link between these two fields is

---

*Corresponding author. Tel.: +39 6551733491; fax: +39 655173252.
E-mail address: fbotta@macchine.uniroma3.it (F. Botta).

[1] This concept was introduced in a Biot's study of a building under seismic loads (1932) [2].

0022-460X/$ - see front matter © 2007 Elsevier Ltd. All rights reserved.
doi:10.1016/j.jsv.2007.04.035

presented. In particular, a relationship between the SRS and the impulse (rise function, rise time) and geometric parameters (thickness of the plate, distance of the measure point from the point load) has been evaluated. The plate model considered is the Reissner–Mindlin plate.[2] It is well known that this model takes into account the shear deformability, unlike the Kirchhoff–Love model. This effect is important as the thickness span or the wavenumber increases, so that to compute the acceleration of a propagation wave, where the eigenmodes at high frequencies must be considered, it cannot be omitted. The aim of this work is to propose a method that can help to find the optimal configuration of the system to reproduce the real SRS in laboratory, reducing the number of trials. Besides, if the loads applied to a plate element of satellite are known, it is possible to calculate the SRS in every point of the plate and chose the best position for sensible electronic components.

2. Eigenfrequencies and eigenmodes of Reissner–Mindlin plates

The theory of Reissner–Mindlin plates is well known [9]. Let $\mathscr{E}$ be the Euclidian ambient space, the plate reference configuration in $\mathscr{E}$ is a right cylinder $\mathscr{C}(\varepsilon)$ of thickness 2ε:

$$\mathscr{C}(\varepsilon)\colon \mathscr{P} \times [-\varepsilon, +\varepsilon] \Rightarrow \mathscr{P} = [0, L_x] \cup [0, L_y]. \tag{1}$$

The displacement vector $\mathbf{u}$ can be decomposed in a vector $\mathbf{v}$ parallel to the middle plane of the plate and another $w\mathbf{e}$ perpendicular to the same plane Fig. 1:

$$\mathbf{u}(\mathbf{p}, \varsigma, t) = w(\mathbf{p}, t)\mathbf{e} + \varsigma\mathbf{v}(\mathbf{p}, t); \quad \mathbf{v} \cdot \mathbf{e} = 0. \tag{2}$$

In order to write these equations in synthetic form it is useful to proceed along the lines of Ref. [10] and use the same terminology:

the mean stress $\mathbf{N}$ and the couple stress $\mathbf{M}$ are defined to be

$$\mathbf{N} = \int_{-\varepsilon}^{+\varepsilon} \mathbf{S}(\mathbf{p}, \zeta, t)\,\mathrm{d}\zeta, \quad \mathbf{M} = \int_{-\varepsilon}^{+\varepsilon} \zeta\mathbf{S}(\mathbf{p}, \zeta, t)\,\mathrm{d}\zeta; \tag{3}$$

the bulk force $\mathbf{b}$ and the bulk couple $\mathbf{c}$ are:

$$\mathbf{b} = \int_{-\varepsilon}^{+\varepsilon} \mathbf{f}(\mathbf{p}, \zeta, t)\,\mathrm{d}\zeta, \quad \mathbf{c} = \int_{-\varepsilon}^{+\varepsilon} \zeta\mathbf{f}(\mathbf{p}, \zeta, t)\,\mathrm{d}\zeta; \tag{4}$$

and the base boundary-traction $\mathbf{n}$ and the boundary couple $\mathbf{m}$ are:

$$\mathbf{n} = \int_{-\varepsilon}^{+\varepsilon} \mathbf{t}(\mathbf{p}, \zeta, t)\,\mathrm{d}\zeta, \quad \mathbf{m} = \int_{-\varepsilon}^{+\varepsilon} \zeta\mathbf{t}(\mathbf{p}, \zeta, t)\,\mathrm{d}\zeta; \tag{5}$$

where $\mathbf{S}$ is the stress tensor, $\mathbf{f}$ are the volume forces, $\mathbf{t}$ is the applied traction at boundary $\partial\mathscr{P}$, $\mathbf{t}^+$ and $\mathbf{t}^-$ are, respectively, the applied traction at upper and lower surfaces.

In addition, the subsequent symbols are defined[3]:

$$\mathbf{P} = \mathbf{I} - \mathbf{e} \otimes \mathbf{e}, \quad \mathbf{Q} = \mathbf{P}(\mathbf{N}\mathbf{e}), \quad \widehat{\mathbf{M}} = \mathbf{P} \boxtimes \mathbf{P}[\mathbf{M}]. \tag{6}$$

With these notations the balance equations can be written in the form [9]

$$\begin{aligned} &-\mathrm{div}(\mathbf{Q}) = b_\zeta + t_\zeta^+ + t_\zeta^-, \\ &-\mathrm{div}(\widehat{\mathbf{M}}) + \mathbf{Q} = \mathbf{P}\mathbf{c} + \varepsilon\mathbf{P}(\mathbf{t}^+ - \mathbf{t}^-), \end{aligned} \tag{7}$$

together with the boundary conditions:

$$\left.\begin{aligned} \mathbf{N}\mathbf{v} &= \mathbf{n}, \\ \mathbf{M}\mathbf{v} &= \mathbf{m}, \end{aligned}\right. \quad \text{on } \partial\mathscr{P}, \tag{8}$$

where $\mathbf{v}$ is the outward unit normal to $\partial\mathscr{P}$ (Fig. 1).

---

[2] A 3D approach furnishes the exact solution but, for some applications, can be very onerous.

[3] Given $A, B, C \in \mathrm{Lin}$, the conjugation product of the ordered pair (A, B) is the fourth-order tensor: $\mathbf{A} \boxtimes \mathbf{B}[\mathbf{C}] = \mathbf{A}\mathbf{C}\mathbf{B}^{\mathrm{T}}$.

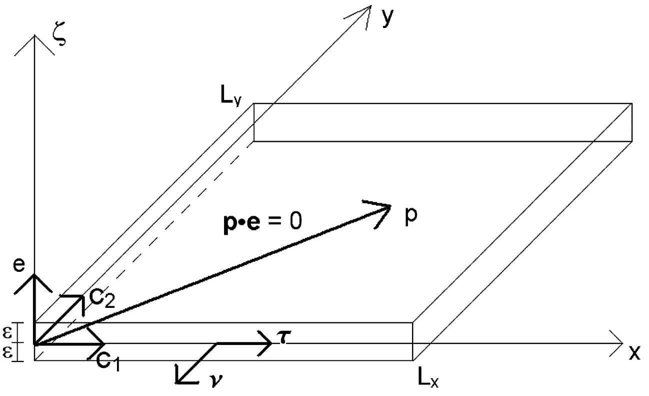

Fig. 1. Plate reference configuration.

The eigenmodes and eigenvalues are obtained from the solution of the free vibration problems

$$\mathbf{f} = -\rho\ddot{\mathbf{u}} = -\rho(\ddot{w}\mathbf{e} + \zeta\ddot{\mathbf{v}}), \tag{9}$$

where ρ denotes the mass density and superposed point the derivative with respect to the time t.

Then from Eqs. (4) and (5):

$$\left.\begin{aligned} &\mathbf{b} = -\rho\textstyle\int_{-\varepsilon}^{+\varepsilon}(\ddot{w}\mathbf{e} + \zeta\ddot{\mathbf{v}}) = -2\varepsilon\rho\ddot{w}\mathbf{e},\\ &\mathbf{c} = -\rho\textstyle\int_{-\varepsilon}^{+\varepsilon}(\zeta\ddot{w}\mathbf{e} + \zeta^2\ddot{\mathbf{v}}) = -\tfrac{2}{3}\varepsilon^3\rho\ddot{\mathbf{v}},\\ &\mathbf{n} = 0,\\ &\mathbf{m} = 0,\\ &\mathbf{t}^+ = \mathbf{0},\\ &\mathbf{t}^- = \mathbf{0}, \end{aligned}\right. \quad \text{on } \mathscr{P} \tag{10}$$

and therefore (7) begins:

$$\begin{aligned} &\operatorname{div}(\mathbf{Q}) = 2\varepsilon\rho\ddot{w},\\ &-\operatorname{div}(\widehat{\mathbf{M}}) + \mathbf{Q} = -\tfrac{2}{3}\varepsilon^3\rho\ddot{\mathbf{v}}. \end{aligned} \tag{11}$$

To write the equilibrium equations in terms of displacements, the constitutive equations for elastic transversely isotropic material, regarding the direction $\mathbf{e}$, must be introduced [11], and the equation that governs free vibrations of Reissner–Mindlin plates is obtained:

$$D\nabla^4\overline{w} + \omega^2\left(\frac{D}{\eta}\rho + \frac{2}{3}\varepsilon^3\rho\right)\nabla^2\overline{w} + \omega^2\left(\frac{2}{3}\varepsilon^3\frac{1}{\eta}\omega^2\rho^2 - 2\varepsilon\rho\right)\overline{w} = 0 \quad \text{on} \quad P, \tag{12}$$

where $D = E(2\varepsilon)^3/(12(1-\nu^2))$ is the flexural rigidity (E the Young's modulus and ν the Poisson's coefficient) and $\eta = k^2G$ is the shear coefficient with $k^2 = 5/6$ [12].

To study the dispersion relations it is sufficient to let [13]:

$$w(x,t) = \cos[\xi(x - ct)], \tag{13}$$

and the resulting dispersion curve is shown in Fig. 2. The dimensionless velocity and wavenumber of the figure are $\overline{c} = c/c_s$ and $\overline{\xi} = \xi h/2\pi$ with $c_s = (G/\rho)^{1/2}$, $G = [E/2(1+\nu)]$ and $h = 2\varepsilon$. It must be observed that for low wavenumbers the three theories: exact 3D, Kirchhoff–Love (classical plate theory) and Reissner–Mindlin (classical plate theory + shear correction), with or without rotary inertia correction, are in good agreement; by increasing ξ the differences between the 3D and Kirchhoff–Love solution are relevant, while it is impossible to detect differences between 3D and the Reissner–Mindlin solution.

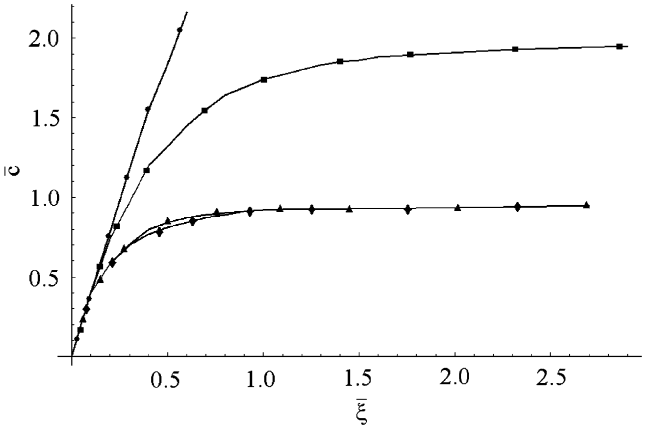

Fig. 2. Dispersion curve: ● = Kirchhoff–Love theory; ■ = Kirchhoff–Love theory + rotary inertia correction; ▲ = Reissner–Mindlin theory; ◆ = Reissner–Mindlin theory + rotary inertia correction or three-dimensional solution (from Ref. [13]).

If it is assumed that the boundary conditions are simply supported edges[4]:

$$\begin{aligned} &w(\mathbf{p}) = 0, \\ &v_\tau(\mathbf{p}) = 0, \\ &\mathbf{M}\boldsymbol{\nu}\cdot\nu = 0, \end{aligned} \tag{15}$$

the analytical expressions for the eigenmodes are:

$$\overline{w}_{mn}(\mathbf{p}) = \sin\left(\frac{m\pi x}{L_x}\right)\sin\left(\frac{n\pi y}{L_y}\right), \tag{16}$$

$$\overline{\mathbf{v}}_{mn}(\mathbf{p}) = -C_{mn}\pi\left\{\begin{matrix} \cos\left(\dfrac{m\pi x}{L_x}\right)\sin\left(\dfrac{n\pi y}{L_y}\right)\dfrac{m}{L_x} \\ \sin\left(\dfrac{m\pi x}{L_x}\right)\cos\left(\dfrac{n\pi y}{L_y}\right)\dfrac{n}{L_y} \end{matrix}\right\}, \tag{17}$$

with $h = 2\varepsilon$ being the plate thickness,

$$\widehat{\omega}_{mn}^{\mathrm{KL}} = \pi^2\left(\sqrt{\frac{D}{\rho h}}\right)\left(\frac{m^2}{L_x^2} + \frac{n^2}{L_y^2}\right)$$

the frequency of vibration of the Kirchhoff–Love plate and[5]

$$C_{mn} = \frac{\left(\dfrac{m\pi}{L_x}\right)^2 + \left(\dfrac{n\pi}{L_y}\right)^2 - \dfrac{\rho\omega_{mn}^2}{\eta}}{\left(\dfrac{m\pi}{L_x}\right)^2 + \left(\dfrac{n\pi}{L_y}\right)^2} = \frac{\widehat{\omega}_{mn}^{\mathrm{KL}}\sqrt{\dfrac{h\rho}{D}} - \dfrac{\rho\omega_{mn}^2}{\eta}}{\widehat{\omega}_{mn}^{\mathrm{KL}}\sqrt{\dfrac{h\rho}{D}}} = 1 - \frac{1}{\eta}\sqrt{\frac{\rho D}{h}}\frac{\omega_{mn}^2}{\widehat{\omega}_{mn}^{\mathrm{KL}}}, \tag{18}$$

---

[4] In the Reissner–Mindlin plate these simply supported boundary conditions are called "hard type", the simply supported boundary conditions of the "soft type" are:

$$\begin{aligned} &w(\mathbf{p}) = 0, \\ &\mathbf{M}\boldsymbol{\nu}\cdot\boldsymbol{\tau} = 0, \\ &\mathbf{M}\boldsymbol{\nu}\cdot\nu = 0, \end{aligned} \tag{14}$$

$\boldsymbol{\tau}$ is the direction tangent to the edge (Fig. 1).

[5] It can be observed that putting $\eta = \infty$ the eigenmodes of the Kirchhoff–Love plate are obtained.

while the expression for the eigenfrequencies is [14,15] [6]:

$$(\omega_{mn})^2 = \frac{1}{2h^3\rho}\left[\sqrt{\frac{\rho h}{D}}\widehat{\omega}_{mn}^{\mathrm{KL}} h^3\eta + 12\eta h + 12D\sqrt{\frac{\rho h}{D}}\widehat{\omega}_{mn}^{\mathrm{KL}} - \sqrt{\left(12\eta h + (\eta h^3 + 12D)\sqrt{\frac{\rho h}{D}}\widehat{\omega}_{mn}^{\mathrm{KL}}\right)^2 - 48h^4\eta\rho(\widehat{\omega}_{mn}^{\mathrm{KL}})^2}\,\right]. \tag{19}$$

3. Propagation of flexural waves

If a load is applied on upper surface

$$\mathbf{t}^+ = g(\mathbf{p})r(t,\tau)[a\mathbf{e} + d_1\mathbf{c}_1 + d_2\mathbf{c}_2]. \tag{20}$$

Using the modal analysis technique and the constitutive equations, the equilibrium equations (7) become:

$$\mathbf{H}\ddot{\mathbf{u}} + \mathbf{L}\mathbf{u} = \mathbf{f} \tag{21}$$

with

$$\mathbf{H} = \begin{bmatrix} \dfrac{h^3\rho}{12} & 0 & 0 \\ 0 & \dfrac{h^3\rho}{12} & 0 \\ 0 & 0 & h\rho \end{bmatrix},$$

$$\mathbf{u} = \begin{Bmatrix} v_x(x,y,t) \\ v_y(x,y,t) \\ w(x,y,t) \end{Bmatrix},$$

$$\mathbf{L} = \begin{bmatrix} -\dfrac{D}{2}\left[2\dfrac{\partial^2}{\partial x^2} + (1-v)\dfrac{\partial^2}{\partial y^2}\right] + h\eta & -\dfrac{D}{2}(1+v)\dfrac{\partial^2}{\partial x\partial y} & h\eta\dfrac{\partial}{\partial x} \\ -\dfrac{D}{2}(1+v)\dfrac{\partial^2}{\partial x\partial y} & -\dfrac{D}{2}\left[2\dfrac{\partial^2}{\partial y^2} + (1-v)\dfrac{\partial^2}{\partial x^2}\right] + h\eta & h\eta\dfrac{\partial}{\partial y} \\ -h\eta\dfrac{\partial}{\partial x} & -h\eta\dfrac{\partial}{\partial y} & -h\eta\left(\dfrac{\partial^2}{\partial x^2} + \dfrac{\partial^2}{\partial y^2}\right) \end{bmatrix},$$

$$\mathbf{f} = \begin{Bmatrix} \dfrac{h}{2}(s_{0x}^+ - s_{0x}^-) \\ \dfrac{h}{2}(s_{0y}^+ - s_{0y}^-) \\ s_{0\varsigma}^+ + s_{0\varsigma}^- \end{Bmatrix}. \tag{22}$$

The displacement vector can be obtained by superposition of normal modes:

---

[6] It is possible to obtain an approximate solution of Eq. (12) ignoring the fourth-order term in ω:

$$\widetilde{\omega}_{mn} = \frac{\widehat{\omega}^{\mathrm{KL}}}{\sqrt{\left[1 - \widehat{\omega}^{\mathrm{KL}}\sqrt{\frac{h\rho}{D}}\left(\frac{D}{h\eta} + \frac{h^2}{12}\right)\right]}}.$$

$$\mathbf{u}(x,y,t)=\sum_{m=1}^{\infty}\sum_{n=1}^{\infty}\beta_{mn}(t)\left\{\begin{matrix}\dfrac{-C_{mn}\pi m}{L_x}\cos\left(\dfrac{m\pi x}{L_x}\right)\sin\left(\dfrac{n\pi y}{L_y}\right)\\ \dfrac{-C_{mn}\pi n}{L_y}\sin\left(\dfrac{m\pi x}{L_x}\right)\cos\left(\dfrac{n\pi y}{L_y}\right)\\ \sin\left(\dfrac{m\pi x}{L_x}\right)\sin\left(\dfrac{n\pi y}{L_y}\right)\end{matrix}\right\}, \tag{23}$$

and substituting in Eq. (21)

$$\ddot{\beta}_{mn}(t)+\omega_{mn}^2\beta_{mn}(t)=\left(\frac{1}{D_{mn}}\right)f_{mn}(t) \tag{24}$$

with

$$\mathbf{U}_{mn}=\left\{\begin{matrix}\dfrac{-C_{mn}\pi m}{L_x}\cos\left(\dfrac{m\pi x}{L_x}\right)\sin\left(\dfrac{n\pi y}{L_y}\right)\\ \dfrac{-C_{mn}\pi n}{L_y}\sin\left(\dfrac{m\pi x}{L_x}\right)\cos\left(\dfrac{n\pi y}{L_y}\right)\\ \sin\left(\dfrac{m\pi x}{L_x}\right)\sin\left(\dfrac{n\pi y}{L_y}\right)\end{matrix}\right\}, \tag{25}$$

$$\int_0^{L_x}\int_0^{L_y}\mathbf{HU_{mn}}\cdot\mathbf{U}_{ij}\,\mathrm{d}x\,\mathrm{d}y=\begin{cases}D_{mn} & \text{if } i=m \text{ and } j=n,\\ 0 & \text{if } i\neq m \text{ or } j\neq n,\end{cases} \tag{26}$$

$$\int_0^{L_x}\int_0^{L_y}\mathbf{LU}_{mn}\cdot\mathbf{U}_{ij}\,\mathrm{d}x\,\mathrm{d}y=\begin{cases}\omega_{mn}^2 D_{mn} & \text{if } i=m \text{ and } j=n,\\ 0 & \text{if } i\neq m \text{ or } j\neq n,\end{cases} \tag{27}$$

$$D_{mn}=\left(\frac{L_xL_y}{4}\right)\left[\rho h+\left(A_{mn}^2+B_{mn}^2\right)\frac{\rho h^3}{12}\right]$$

and

$$f_{mn}(t)=\int_0^{L_x}\int_0^{L_y}\mathbf{f}\cdot\mathbf{U}_{mn}\,\mathrm{d}x\,\mathrm{d}y. \tag{28}$$

The function $\beta_{mn}(t)$ can be obtained by the solution of Eq. (24), together with initial conditions:

$$\begin{aligned}\beta_{mn}(0)&=\int_0^{L_x}\int_0^{L_y}\mathbf{u}(x,y,0)\cdot\mathbf{U}_{mn}(x,y)\,\mathrm{d}x\,\mathrm{d}y,\\ \dot{\beta}_{mn}(0)&=\int_0^{L_x}\int_0^{L_y}\dot{\mathbf{u}}(x,y,0)\cdot\mathbf{U}_{mn}(x,y)\,\mathrm{d}x\,\mathrm{d}y.\end{aligned} \tag{29}$$

Substituting the $\beta_{mn}(t)$ function in Eq. (25) the displacement $\mathbf{u}(x,y,\zeta,t)$ is obtained. In the following only loads along the **e** direction, of intensity P, time function $g(t)$ and applied area $[0,e_x]\cup[0,e_y]$ (Figs. 3 and 4) will be considered so that

$$\mathbf{f}=\left\{\begin{matrix}0\\0\\ g(t)\dfrac{P}{e_xe_y}r(x,y)\end{matrix}\right\}. \tag{30}$$

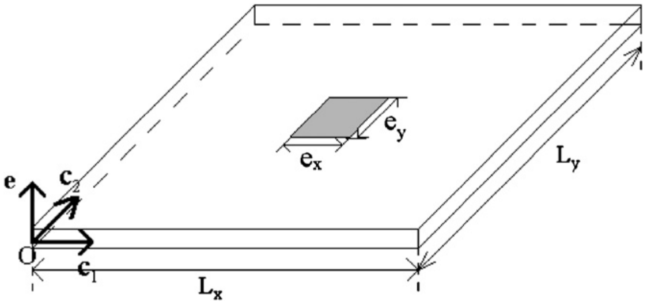

Fig. 3. Surface load.

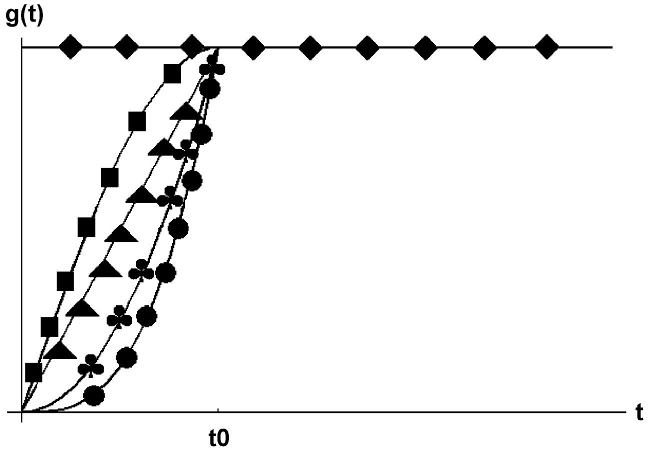

Fig. 4. Type of impulses: ▲ = linear; ♣ = quadratic; • = cubic; ■ = sin; ◆ = step.

Introducing:

$$r(x,y) = \left[H\left(x - \frac{L_x}{2} + \frac{e_x}{2}\right) - H\left(x - \frac{L_x}{2} - \frac{e_x}{2}\right)\right] \times \left[H\left(y - \frac{L_y}{2} + \frac{e_y}{2}\right) - H\left(x - \frac{L_y}{2} - \frac{e_y}{2}\right)\right] \tag{31}$$

and

$$z_{mn} = \int_0^{L_x} \int_0^{L_y} r(x,y) \sin\left(\frac{m\pi x}{L_x}\right) \sin\left(\frac{n\pi y}{L_y}\right) \mathrm{d}x\,\mathrm{d}y \tag{32}$$

(H is the Heaviside function) Eq. (28) begins:

$$f_\zeta(t) = f_{mn}(t) = \frac{P}{e_x e_y} z_{mn} g(t). \tag{33}$$

In Fig. 5 there is an example of propagation of flexural waves in plate under step load.

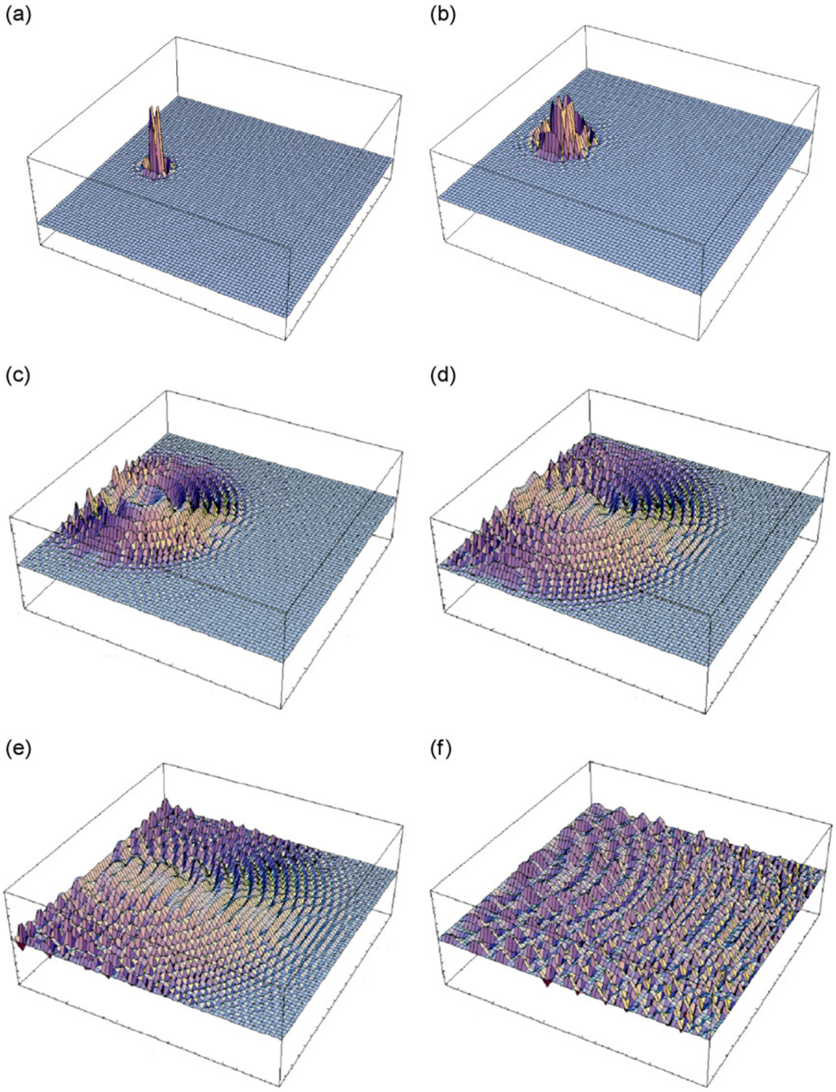

Fig. 5. Propagation of flexural waves in plate under step load.

3.1. Step load

The time function $g(t)$ is

$$g(t) = H(t), \tag{34}$$

thus

$$f_{mn}(t) = \frac{P}{e_x e_y} z_{mn} H(t), \tag{35}$$

and

$$\beta_{mn}(t) = \frac{P z_{mn}}{e_x e_y D_{mn}} \frac{2 \sin\left(\frac{\omega_{mn} t}{2}\right)^2}{\omega_{mn}^2},$$
$$\ddot{\beta}_{mn}(t) = \frac{P z_{mn}}{e_x e_y D_{mn}} \cos(\omega_{mn} t).$$

3.2. *n*-Order curve

In this case

$$g(t) = \left(\frac{t}{t_0}\right)^n - \left[\left(\frac{t}{t_0}\right)^n - 1\right] H(t - t_0), \tag{36}$$

where t_0 is the *rise-time* (Fig. 4). In the following there are the solutions for $n = 1, 2, 3$:

$$n = 1 \quad \begin{aligned} \beta_{mn}(t) &= \begin{cases} \dfrac{Pz_{mn}}{e_x e_y D_{mn}} \dfrac{-\sin(\omega_{mn}t) + \omega_{mn}t}{t_0\omega_{mn}^3}, & t < t_0, \\[2ex] \dfrac{Pz_{mn}}{e_x e_y D_{mn}} \dfrac{-\sin(\omega_{mn}t) + \sin[\omega_{mn}(t - t_0)] + t_0\omega_{mn}}{t_0\omega_{mn}^3}, & t > t_0, \end{cases} \\ \ddot{\beta}_{mn}(t) &= \begin{cases} \dfrac{Pz_{mn}}{e_x e_y D_{mn}} \dfrac{\sin(\omega_{mn}t)}{t_0\omega_{mn}}, & t < t_0, \\[2ex] \dfrac{Pz_{mn}}{e_x e_y D_{mn}} \dfrac{\sin(\omega_{mn}t) - \sin[\omega_{mn}(t - t_0)]}{t_0\omega_{mn}}, & t > t_0; \end{cases} \end{aligned} \tag{37}$$

$$n = 2 \quad \begin{aligned} \beta_{mn}(t) &= \begin{cases} \dfrac{Pz_{mn}}{e_x e_y D_{mn}} \dfrac{-2 + 2\cos(\omega_{mn}t) + \omega_{mn}^2 t^2}{t_0^2\omega_{mn}^4}, & t < t_0, \\[2ex] \dfrac{Pz_{mn}}{e_x e_y D_{mn}} \dfrac{2\{\cos(\omega_{mn}t) - \cos[\omega_{mn}(t - t_0)]\}}{t_0^2\omega_{mn}^4} & \\ \quad + \dfrac{Pz_{mn}}{e_x e_y D_{mn}} \dfrac{\omega_{mn}t_0\{2\sin[\omega_{mn}(t - t_0)] + \omega_{mn}t_0\}}{t_0^2\omega_{mn}^4}, & t > t_0, \end{cases} \\ \ddot{\beta}_{mn}(t) &= \begin{cases} \dfrac{Pz_{mn}}{e_x e_y D_{mn}} \dfrac{2[1 - \cos(\omega_{mn}t)]}{t_0^2\omega_{mn}^2}, & t < t_0, \\[2ex] \quad - \dfrac{Pz_{mn}}{e_x e_y D_{mn}} \dfrac{2\{\cos(\omega_{mn}t) - \cos[\omega_{mn}(t - t_0)]\}}{t_0^2\omega_{mn}^2} & \\ \quad - \dfrac{Pz_{mn}}{e_x e_y D_{mn}} \dfrac{\omega_{mn}t_0 \sin[\omega_{mn}(t - t_0)]}{t_0^2\omega_{mn}^2}, & t > t_0; \end{cases} \end{aligned} \tag{38}$$

$$n = 3 \quad \begin{aligned} \beta_{mn}(t) &= \begin{cases} \dfrac{Pz_{mn}}{e_x e_y D_{mn}} \dfrac{6\sin(\omega_{mn}t) - 6\omega_{mn}t + \omega_{mn}^3 t^3}{t_0^3\omega_{mn}^5}, & t < t_0, \\[2ex] \dfrac{Pz_{mn}}{e_x e_y D_{mn}} \dfrac{6\sin(\omega_{mn}t) - 6\omega_{mn}t_0\cos[\omega_{mn}(t - t_0)]}{t_0^3\omega_{mn}^5} & \\ \quad + \dfrac{Pz_{mn}}{e_x e_y D_{mn}} \dfrac{t_0^3\omega_{mn}^3 + 3\sin[\omega_{mn}(t - t_0)](-2 + t_0^2\omega_{mn}^2)}{t_0^3\omega_{mn}^5}, & t > t_0, \end{cases} \\ \ddot{\beta}_{mn}(t) &= \begin{cases} \dfrac{Pz_{mn}}{e_x e_y D_{mn}} \dfrac{6[-\sin(\omega_{mn}t) + \omega_{mn}t]}{t_0^3\omega_{mn}^3}, & t < t_0, \\[2ex] \dfrac{Pz_{mn}}{e_x e_y D_{mn}} \dfrac{-6\sin(\omega_{mn}t) + 6\sin[\omega_{mn}(t - t_0)]}{t_0^3\omega_{mn}^3} & \\ \quad + \dfrac{Pz_{mn}}{e_x e_y D_{mn}} \dfrac{-3t_0\omega_{mn}\{-2\cos[\omega_{mn}(t - t_0)]\}}{t_0^3\omega_{mn}^3} & \\ \quad + \dfrac{Pz_{mn}}{e_x e_y D_{mn}} \dfrac{+\omega_{mn}t_0\sin[\omega_{mn}(t - t_0)]}{t_0^3\omega_{mn}^3}, & t > t_0. \end{cases} \end{aligned} \tag{39}$$

3.3. Sine-load

For the sine-load

$$g(t) = \sin\left[\frac{\pi}{2}\left(\frac{t}{t_0}\right)\right] - \left(\sin\left[\frac{\pi}{2}\left(\frac{t}{t_0}\right)\right] - 1\right)H(t - t_0) \tag{40}$$

and the solutions are:

$$\beta_{mn}(t) = \begin{cases} \dfrac{Pz_{mn}}{e_x e_y D_{mn}} \dfrac{2\pi t_0 \sin(\omega_{mn} t) - 4\omega_{mn} t_0^2 \sin\left(\dfrac{\pi t}{2t_0}\right)}{\pi^2 \omega_{mn} - 4\omega_{mn}^3 t_0^2}, & t < t_0, \\ \dfrac{Pz_{mn}}{e_x e_y D_{mn}} \dfrac{\pi^2\{1 - \cos[(t - t_0)\omega_{mn}]\}}{\omega_{mn}^2(\pi - 2\omega_{mn} t_0)(\pi + 2\omega_{mn} t_0)} & \\ \quad + \dfrac{Pz_{mn}}{e_x e_y D_{mn}} \dfrac{2\omega_{mn} t_0[-\pi \sin(\omega_{mn} t) + 2\omega_{mn} t_0]}{\omega_{mn}^2(\pi - 2\omega_{mn} t_0)(\pi + 2\omega_{mn} t_0)}, & t > t_0, \end{cases}$$

$$\ddot{\beta}_{mn}(t) = \begin{cases} \dfrac{Pz_{mn}}{e_x e_y D_{mn}} \dfrac{\pi \sin\left(\dfrac{\pi t}{2t_0}\right) - 2\omega_{mn} t_0 \sin(\omega_{mn} t)}{\pi^2 - 4\omega_{mn}^2 t_0^2}, & t < t_0, \\ \dfrac{Pz_{mn}}{e_x e_y D_{mn}} \dfrac{\pi\{\pi \cos[(t - t_0)\omega_{mn}] - 2\omega_{mn} t_0 \sin(\omega_{mn} t)\}}{\pi^2 - 4\omega_{mn}^2 t_0^2}, & t > t_0. \end{cases} \tag{41}$$

4. Numerical results and discussions

In order to validate the method, a comparison with published results, derived by other methods, has been made. In Ref. [8] Weaver and Pao have developed a 3D solution with following parameters: $E = 67.8\,\mathrm{GPa}$, $\nu = 0.21$, $\rho = 2300\,\mathrm{kg/m^3}$. The load is a step pulse of intensity $-3.46\,\mathrm{N}$. Fig. 6 shows that the two solutions, with the same values for the Reissner–Mindlin plate model, agree well in the time interval. Proceeding to study the typical aerospace element, an aluminum plate with $E = 73\,\mathrm{GPa}$, $\nu = 0.32$, $\rho = 2770\,\mathrm{kg/m^3}$ has been taken into account. In Figs. 7–13 the acceleration versus time, the amplitude of the coefficient of the acceleration $\ddot{\beta}_{mn}$ as a function of proper frequencies f_{mn}, and the SRS for different rise times and rise functions are reported. The distance between the measurement and the load point is approximately 10 cm. It is possible to observe that, for a fixed rise function, the increase of the rise time reduces the values of the acceleration amplitude in all the range of frequencies and therefore also the values of the acceleration versus time. It must be noticed that as the time increases, the percentage influence of the low-frequency components grows, and this effect becomes more evident with increasing values of t_0. The correlated SRS shows that there is a reduction only at high

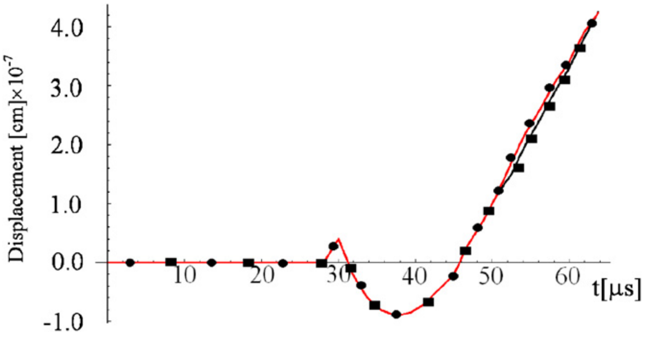

Fig. 6. Comparison between 3D(■) and Reissner–Mindlin (•) solution (from Ref. [8]).

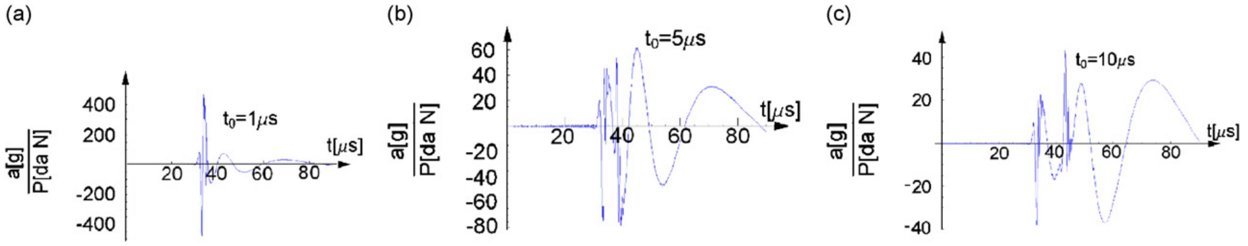

Fig. 7. Linear ramp: acceleration versus time.

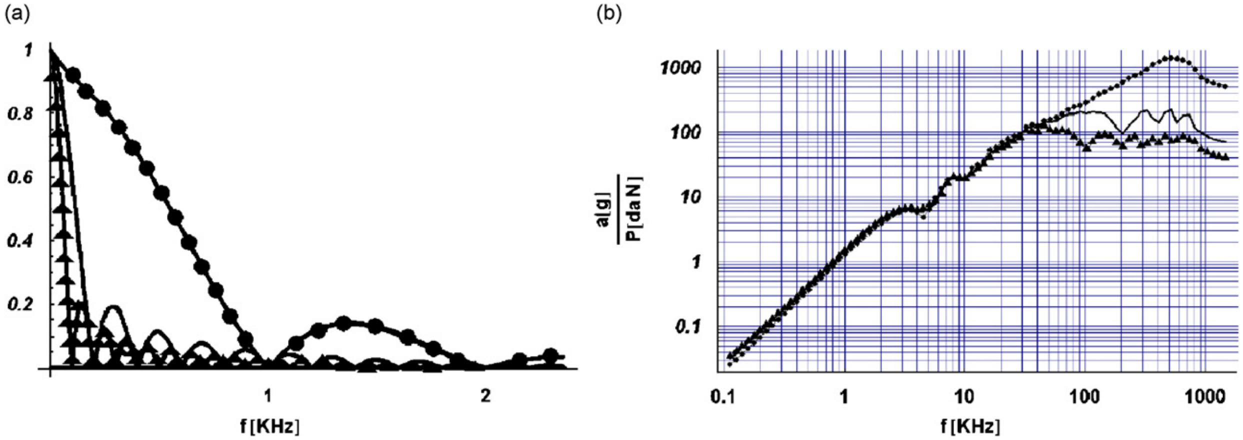

Fig. 8. Linear ramp: $\ddot{\beta}_{mn}(f_{mn})$ (a), SRS (b) • ⇒ $t_0 = 1\,\mu\text{s}$; —— ⇒ $t_0 = 5\,\mu\text{s}$; ▲ ⇒ $t_0 = 10\,\mu\text{s}$.

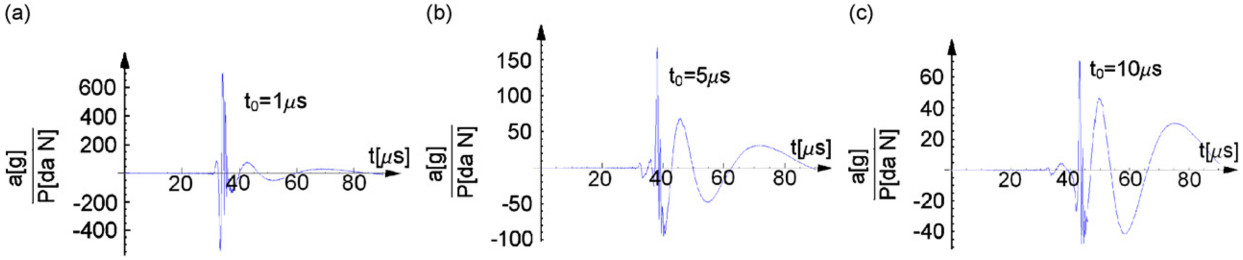

Fig. 9. Quadratic ramp: acceleration versus time.

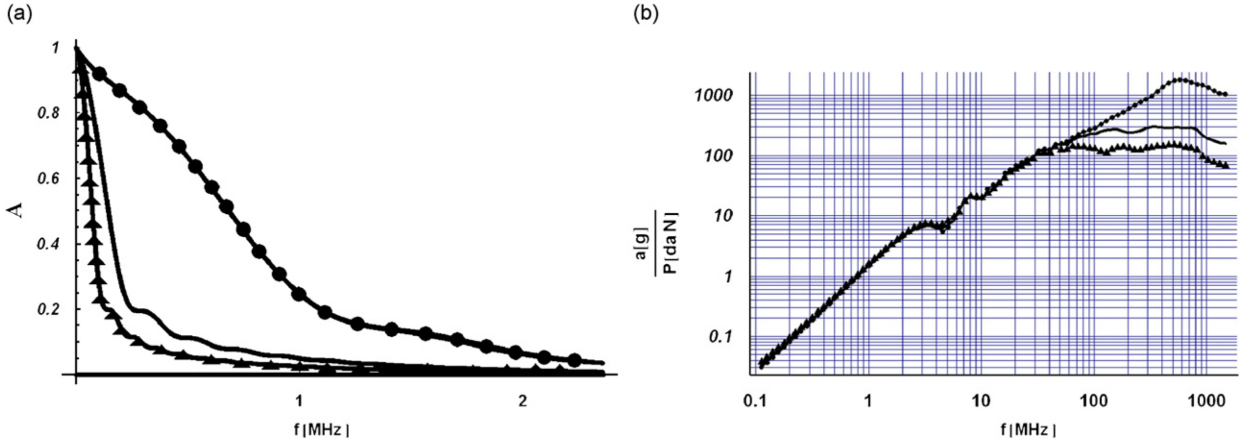

Fig. 10. Quadratic ramp: $\ddot{\beta}_{mn}(f_{mn})$ (a), SRS (b) • ⇒ $t_0 = 1\,\mu\text{s}$; —— ⇒ $t_0 = 5\,\mu\text{s}$; ▲ ⇒ $t_0 = 10\,\mu\text{s}$.

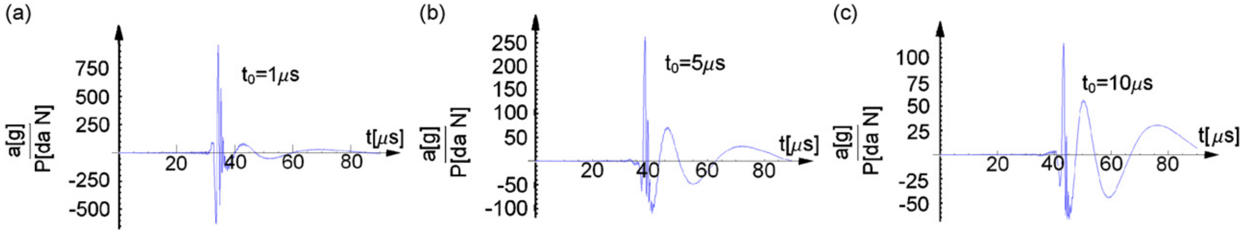

Fig. 11. Cubic ramp: acceleration versus time.

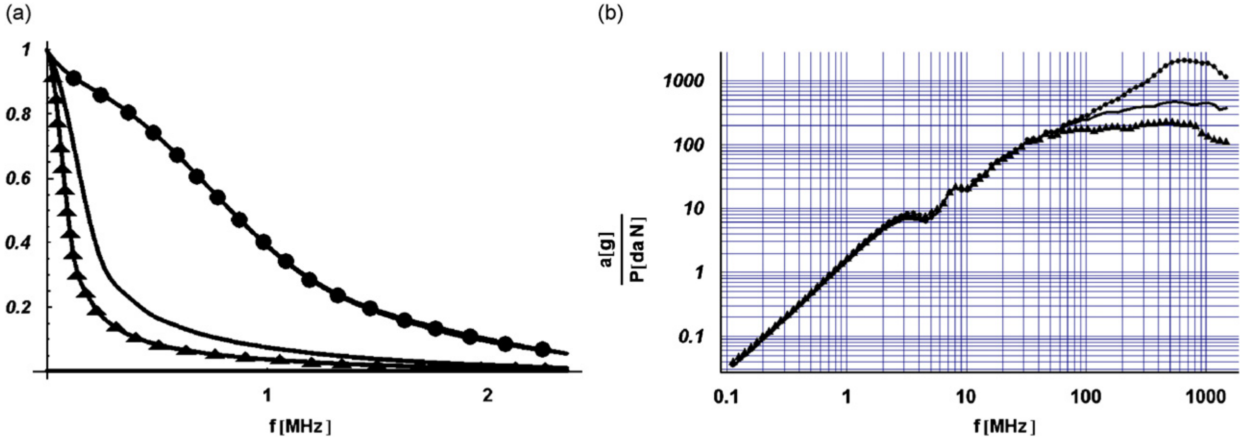

Fig. 12. Cubic ramp: $\ddot{\beta}_{mn}(f_{mn})$ (a), SRS (b) • ⇒ $t_0 = 1\,\mu\text{s}$; —— ⇒ $t_0 = 5\,\mu\text{s}$; ▲ ⇒ $t_0 = 10\,\mu\text{s}$.

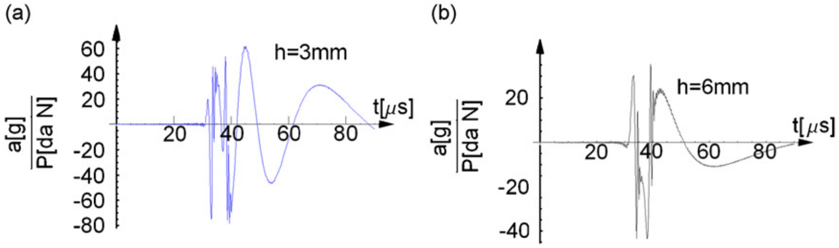

Fig. 13. Influence of thickness—linear ramp ($t_0 = 5$): acceleration versus time.

frequencies. In the case of the quadratic and cubic ramp the spectrum curve of $\ddot{\beta}_{mn}$ is similar to a rectangular hyperbola and the vertex goes towards the origin of the axes as t_0 increases. The influence of the thickness h and the distance Δr on SRS is reported in Figs. 14 and 15.It can be seen that the values decrease, when h or Δr is increased, in all the range of frequencies considered. In Figs. 16–18 there is the comparison between the SRS due to the different rise function and in different rise times. It is possible to observe that, in all the rise times considered, when order of the curve increases the values at high frequencies grow.

5. Conclusions

In this paper the method of expansion in normal modes has been applied to study the response of a Reissner–Mindlin plate under impulse loads. In particular the influence of impulse parameters and geometric characteristics of the plate on the Shock Response Spectrum (SRS) has been studied. The results show that by

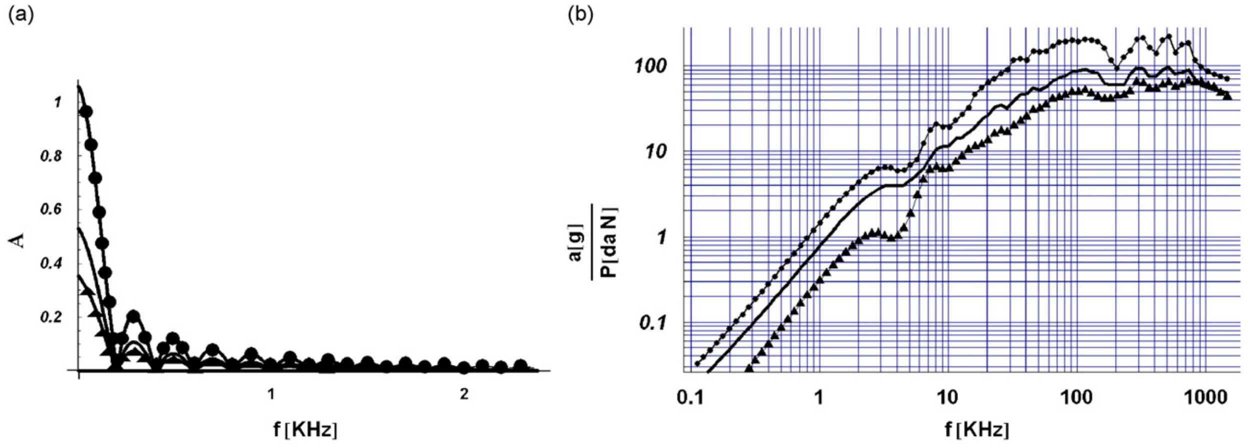

Fig. 14. Influence of thickness—linear ramp ($t_0 = 5$): $\ddot{\beta}_{mn}(f_{mn})$ (a), SRS (b) • ⇒ $h = 3\,\text{mm}$; —— ⇒ $h = 6\,\text{mm}$; ▲ ⇒ $h = 9\,\text{mm}$.

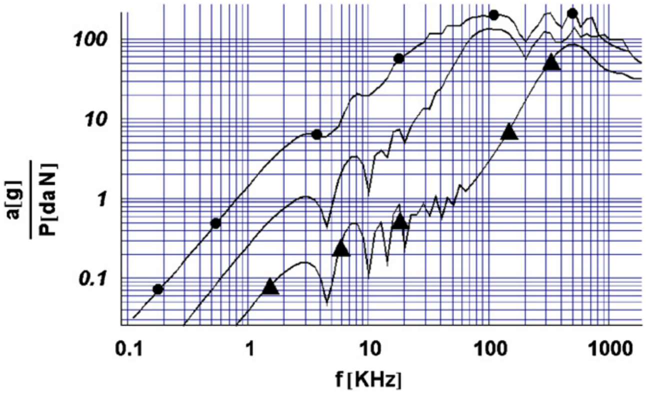

Fig. 15. Influence of distance from the impact point (linear ramp $t_0 = 5\,\mu\text{s}$) • ⇒ $\Delta r = 10\,\text{cm}$; —— ⇒ $\Delta r = 20\,\text{cm}$; ▲ ⇒ $\Delta r = 30\,\text{cm}$.

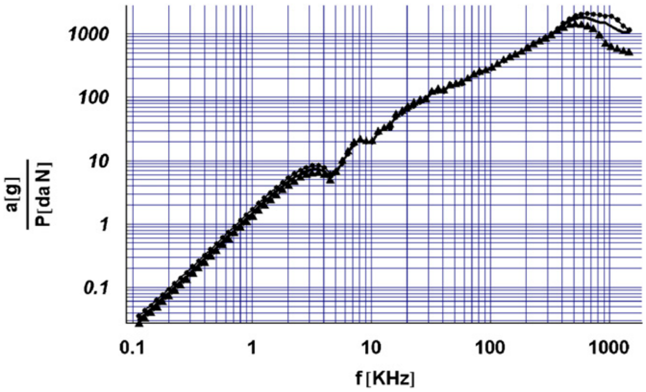

Fig. 16. Influence of the ramp type: $t_0 = 1\,\mu\text{s}$; • ⇒ cubic; —— ⇒ quadratic; ▲ ⇒ linear.

increasing the rise time the values of the SRS to high frequencies are reduced, while the augment of the thickness h or of the distance from the impulse point reduces the values of the SRS in all the frequency range. The SRS at low frequencies does not depend significantly on the variation of the rise function impulse considered (linear, quadratic and cubic).

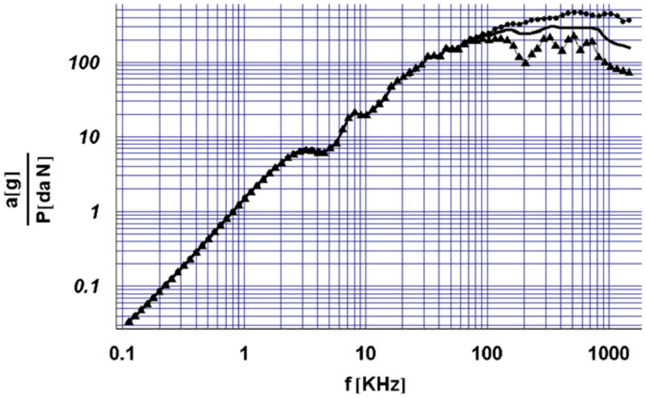

Fig. 17. Influence of the ramp type $t_0 = 5\,\mu s$ • ⇒ cubic; —— ⇒ quadratic; ▲ ⇒ linear.

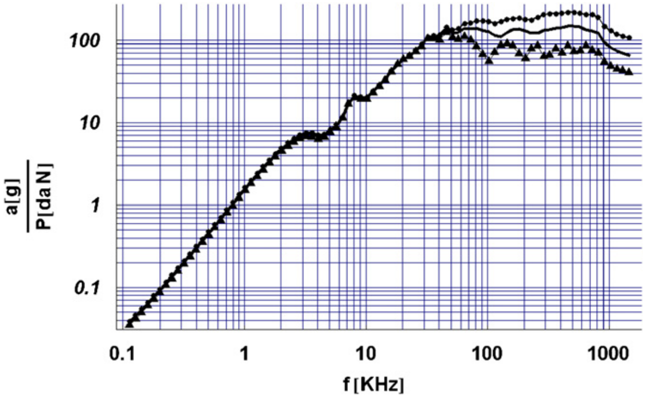

Fig. 18. Influence of the ramp type $t_0 = 10\,\mu s$ • ⇒ cubic; —— ⇒ quadratic; ▲ ⇒ linear.

Acknowledgments

The authors thank the two anonymous reviewers for helpful and their very constructive comments.

Appendix. SRS

The SRS is the maximum absolute acceleration response of a single degree of freedom (SDOF) to the application of the acceleration time history to its base [16], plotted over the specified frequency range and with a constant quality factor $Q = 1/2\delta$, where δ is a viscous damping ratio. In this study, the acceleration applied to the base is the vertical acceleration of an upper surface point of the plate (Fig. 3).

The equilibrium equation of a SDOF (Fig. A.1) is

$$m\ddot{x}_i(\omega_i, t) + c_i[\dot{x}_i(\omega_i, t) - \dot{u}(t)] + k_i[x_i(\omega_i, t) - u(t)] = 0 \tag{42}$$

and the acceleration solution [3]

$$\begin{aligned}\ddot{x}_i(\omega_i, t) = 2\varsigma\omega_i \int_0^t \ddot{u}(\tau)\mathrm{e}^{-\varsigma\omega_i(t-\tau)} \cos[\omega_{d_i}(t-\tau)]d\tau \\ + \left[\frac{\omega_i^2(1-2\varsigma^2)}{\omega_{d_i}}\right] \int_0^t \ddot{u}(\tau)\mathrm{e}^{-\varsigma\omega_i(t-\tau)} \sin[\omega_{d_i}(t-\tau)]\,\mathrm{d}\tau.\end{aligned} \tag{43}$$

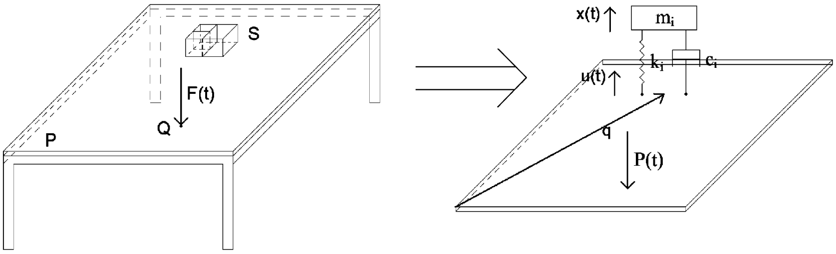

Fig. A.1. SRS construction.

If the modal analysis is applied, $\varphi_j(\mathbf{q})$ are the eigenfunctions and $\alpha_j(t)$ their coefficients, the expression of the vertical displacement $w(\mathbf{q}, t)$ in a point $\mathbf{q}$ of the plate can be written:

$$w(\mathbf{q}, t) = \sum_{j=1}^{N} \alpha_j(t)\varphi_j(\mathbf{q}). \tag{44}$$

By differentiating Eq. (44) two times with respect to t and substituting it in Eq. (43) the acceleration of the mass m_i is obtained:

$$\ddot{x}_i(\omega_i, t) = \sum_{j=1}^{N} \varphi_j(\mathbf{q})q_j(\omega_i, t) \tag{45}$$

with

$$q_j(\omega_i, t) = \int_0^t \ddot{\alpha}_j(\tau)\mathrm{imp}(\omega_i, t-\tau)\,\mathrm{d}\tau \tag{46}$$

and

$$\begin{aligned}\mathrm{imp}(\omega_i, t-\tau) = {} & 2\varsigma\omega_i \mathrm{e}^{-\varsigma\omega_i(t-\tau)}\cos[\omega_{d_i}(t-\tau)]d\tau \\ & + \left[\frac{\omega_i^2(1-2\varsigma^2)}{\omega_{d_i}}\right]\mathrm{e}^{-\varsigma\omega_i(t-\tau)}\sin[\omega_{d_i}(t-\tau)]\,\mathrm{d}\tau.\end{aligned} \tag{47}$$

The maximum value of the function $\ddot{x}_i(\omega_i, t)$ versus t furnishes the SRS in the point $\mathbf{q}$ at the frequency f_i. Varying the frequency f_i the diagram of the SRS in the point $\mathbf{q}$ is obtained(Fig. A.1).

References

[1] C.J. Moenig, Pyrotechnic shock failures, *Proceedings of the Eighth Aerospace Testing Seminar*, 1984, pp. 95–109.
[2] K.G. McConnel, *Vibration Testing—Theory and Practice*, Wiley, New York, 1995.
[3] C.M. Harris, *Shock and Vibration Handbook*, McGraw-Hill, New York, 1995.
[4] D.S. Steinberg, *Vibration Analysis for Electronic Equipment*, Wiley, New York, 2000.
[5] E. Filippi, H. Attouman, C. Conti, Pyroshock simulating using the alcatel ETCA test facility, Launch Vehicle Vibrations. First European Conference, CNES Toulose, 1999.
[6] K.Y. Chang, JPL pyro shock test approach and results, *Proceeding's of the Ninth Aerospace Testing Seminar*, Los Angeles, CA, October 1985.
[7] A.N. Ceranoglu, Y. Pao, Propagation of elastic pulses and acoustic emission in a plate, part I: theory, part II: epicentral response, part III: general response, *Journal of Applied Mechanics* 48 (1981) 125–147.
[8] R.L. Weaver, Y. Pao, Axisymmetric elastic waves excited by a point source in a plate, *Journal of Applied Mechanics* 49 (1982) 821–836.
[9] K.M. Liew, C.M. Wang, Y. Xiang, *Vibration of Mindlin Plates*, Elsevier, Amsterdam, 1998.
[10] A. Di Carlo, P. Podio-Guidugli, W.O. Williams, Shell with thickness distension, *International Journal of Solids Structures* 38 (2001) 1201–1225.
[11] P. Podio-Guidugli, A primer in elasticity, *Journal of Elasticity* 58 (2000).
[12] R.D. Mindlin, Influence of rotatory inertia and shear on flexural motion of isotropic, elastic plates, *Journal of Applied Mechanics* 18 (1951) 31–38.

[13] K.F. Graff, *Wave Motion in Elastic Solids*, Dover, New York, 1991.
[14] C.M. Wang, S. Kitipornchai, Frequency relationship between Levinson plates and classical thin plates, *Mechanics of Research Communication* 26 (1999) 687–692.
[15] J.N. Reddy, C.M. Wang, An overview of the relationships between solutions of the classical and shear deformation plate theories, *Composites Science and Technology* 60 (2000) 2327–2335.
[16] NASA Technical Standard, *Pyroshock Test Criteria*, NASA-STD-7003, 1999.